# Automated optical liquid film thickness measurement method

Cite as: Review of Scientific Instruments **69**, 4205 (1998); https://doi.org/10.1063/1.1149232
Submitted: 09 June 1998 • Accepted: 15 September 1998 • Published Online: 02 December 1998

**T. A. Shedd and T. A. Newell**



# Automated optical liquid film thickness measurement method

T. A. Shedd[a] and T. A. Newell
*Department of Mechanical and Industrial Engineering, University of Illinois, Urbana, Illinois 61801*

(Received 9 June 1998; accepted for publication 15 September 1998)

A nonintrusive, automated, optical film thickness measurement technique has been developed to be used with a wide range of fluids and flow configurations. In this method, light is reflected from the surface of a liquid film flowing over a transparent wall. This reflected light generates an image on the outside of the wall which is captured and digitized using a charge coupled device camera and framegrabber card in a desktop computer. The image is processed to determine the positions of the reflected light rays, with which the film thickness is calculated. The entire process is automated, allowing for the collection of 600 data points in about 4 min using a personal computer with a 486 microprocessor. Film thicknesses on the order of 0.01 mm may be determined using inexpensive components, with the possibility of greater precision using more advanced imaging equipment. An automated calibration procedure allows for the determination of the necessary physical parameters, so the index of refraction of the test fluid or the test section wall need not be known *a priori*. Static liquid measurements agree to within 2.2% of measurements made using the needle-contact method. Film thickness data are presented for both round and square test sections operating under annular, two-phase flow conditions with air and water. © *1998 American Institute of Physics.*
[S0034-6748(98)02012-7]

## I. INTRODUCTION

The modeling and characterization of thin liquid film flow is of importance to many applications, including steam power generation, crude oil delivery and refinement, chemical processing, and refrigeration systems. Many methods for measuring the thickness of thin liquid films have been developed, the majority of which are designed for use with water due to its conductivity. Contact needles,[1–5] conduction probes,[1,2,6–19] and capacitive sensors[3,18–28] are representative of this class. Other successful methods incorporate light absorption,[29–32] microwave absorption,[33] laser-induced fluorescence,[34,35] or external light reflection.[36]

The use of total internal reflection of light to measure liquid films has been proposed and investigated by Than *et al.*,[37] Yu *et al.*,[38] Evers and Jackson,[39] and Hurlburt and Newell.[40] The method presented here is an inexpensive, nonintrusive measurement system based on the work of Hurlburt and Newell and differs from previous approaches primarily in the delivery of light to the liquid and in the detection of the reflected light. Light emitting diffusely from a point source on the outside of a transparent pipe or channel wall is reflected via total internal reflection at the vapor–liquid interface creating an image of light reflected from the liquid surface on the outside of the pipe or channel wall. This image is then acquired using a charge coupled device (CCD) camera, digitized by a framegrabber board, and processed using custom software to produce a film thickness measurement that is accurate to within 0.01 mm or better. Average film thicknesses ranging from below 0.01 mm to a thickness approximately equal to the thickness of the wall supporting the flow can be measured. The measurement apparatus is easily moved to different points in the flow system, and is computer controlled and operated, allowing for the measurement of large numbers of data points in a short time.

Current applications of this method include the study of annular and stratified two-phase, horizontal flows in circular, square, and triangular pipes with 3 to 4 $cm^2$ cross-sectional areas.[41] Figure 1 illustrates some of the primary characteristics of this type of flow. Another research group has successfully applied the basic technique to the study of the thickness of a liquid fuel film sprayed on a wall surface.[42]

## II. THEORY OF MEASUREMENT BY TOTAL INTERNAL REFLECTION

### A. Determining film thickness

Figure 2 displays the simulated results of rays leaving a point source diffusely from the outer surface of a transparent wall and interacting with the wall medium ($n=1.5$), liquid (water, $n=1.33$), and air ($n=1.00$). The amount of light reflected (or transmitted) at each interface can be determined from Fresnel's relations, given here as

$$r_{\mathrm{TE}}=\frac{\cos\theta-\sqrt{n^2-\sin^2\theta}}{\cos\theta+\sqrt{n^2-\sin^2\theta}} \tag{1}$$

for the transverse electric mode of propagation, and

$$r_{\mathrm{TM}}=\frac{n^2\cos\theta-\sqrt{n^2-\sin^2\theta}}{n^2\cos\theta+\sqrt{n^2-\sin^2\theta}} \tag{2}$$

for the transverse magnetic mode, where $n=n_2/n_1$ is the ratio of the two indices of refraction and $\theta$ is the angle between the incident light and the normal of the interface. As can be seen from these equations, a small amount of energy is reflected even at normal incidence ($\theta=0$). When $n_2$

[a]Electronic mail: shedd@uiuc.edu

 

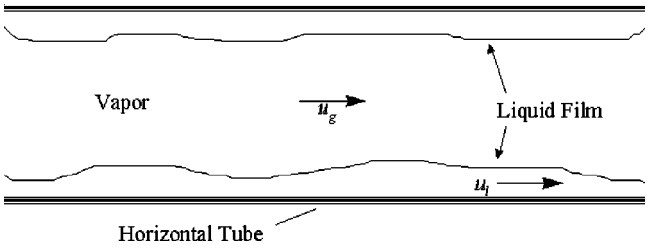


FIG. 1. Schematic of two-phase vapor-liquid flow.

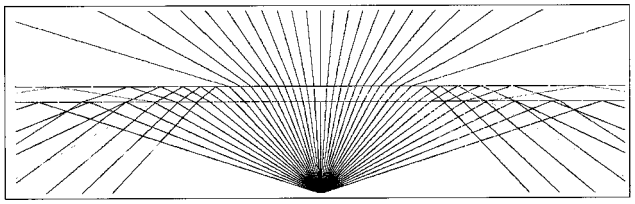

FIG. 2. Simulation of total internal reflection when light rays travel through glass ($n=1.5$) into water ($n=1.33$).

$<n_1$, as is the case at the wall–liquid and liquid–air interfaces in Fig. 2, an angle of incidence will occur for which

$$\sqrt{n^2-\sin^2\theta}=0$$

and Eqs. (1) and (2) both reduce to $r=1$. At this angle of incidence, called the critical angle ($\theta_c$), all of the incident light is reflected. Light arriving at an interface with an angle greater than the critical angle will also be completely reflected, though the Fresnel equations become complex, indicating a phase shift occurs. The Fresnel relations show that when light is incident at the critical angle,

$$\theta_c=\sin^{-1}\frac{n_2}{n_1}, \tag{3}$$

where $n_2$ is the index of refraction of the rarer medium and $n_1$ is the index of refraction of the denser medium. For the situation simulated in Fig. 2, the critical angle at the air–water interface is 48.8° and the critical angle at the water–glass interface is 62.5°.

Figure 3 shows the geometrical relationships needed to determine the thickness of a liquid film. Important dimensions are $t_l$ and $t_w$, the liquid and wall thicknesses, the critical angles of the vapor–liquid interface, $\theta_{cvl}$, and the vapor-wall interface, $\theta_{cvw}$, and the linear distances along the outer test section wall, $x_{\mathrm{dry}}$ and $x_l$. The thickness of a thin liquid film on the wall may be calculated as

$$t_l=\frac{x}{2\tan\theta_{cvl}}-\frac{x_{\mathrm{dry}}}{2\tan\theta_{cvl}}, \tag{4}$$

where

$$x_{\mathrm{dry}}=2t_w\tan\theta_{cvw}.$$

$x_{\mathrm{dry}}$ is the total linear distance that the ray travels while inside the wall medium and is a constant for a given wall material and thickness.

Thus, since $x_{\mathrm{dry}}$ and $\theta_{cvl}$ are constants, a linear relationship exists between the film thickness and the position at which the first fully reflected ray reaches the outer wall surface.

### B. Locating the first fully reflected ray

Central to the calculation of the film thickness is the measurement of the distance between the light source and the point where the first fully reflected ray returns to the outer surface of the wall, as this is the only ray which reflects from the vapor–liquid interface at the critical angle. Looking again at the Fresnel equations, Eqs. (1) and (2), the total percentage of incident light reflected from an interface remains quite small until the angle of incidence approaches the critical angle, whereupon the reflected light intensity increases rapidly. Hence, the intensity of light reflected back to the outer surface of the test section wall will be very low near the light source, but will increase rapidly some distance away from the source as light begins to be strongly reflected back to the outer wall surface. The region where the light intensity increases most rapidly corresponds closely to the location where the first fully reflected light ray returns to the outer surface of the wall. (Note that this is not the location of greatest intensity within the reflected image.) Therefore, an image of the reflected light may be analyzed to determine the point where the change in the light intensity is greatest. The distance between the light source and the point where the first fully reflected ray returns to the outer wall surface may then be determined.

As an additional benefit, using the slope of the light intensity profile reduces sensitivity to background light and fouling of the test section wall, while removing any direct dependence on absolute light intensities, thus simplifying calibration and use of this measurement method.

### C. The experimental setup

The experimental system must perform three primary functions: the generation of diffuse light rays from a point source, the capture of light reflected from the liquid surface, and the analysis of the reflected light rays to determine the thickness of the liquid. Figure 4 shows a schematic diagram of a measurement configuration. Other configurations are described by Shedd[41] as well as Hurlburt and Newell.[40]

A relatively small amount of light is necessary to generate a reflected image of adequate brightness. Thus, for simplicity and economy, light is generated by a high-brightness light emitting diode (LED) on the outside of a test section. The diffusing lens of the LED (the rounded top) is removed down to a point very near the light generating element. To

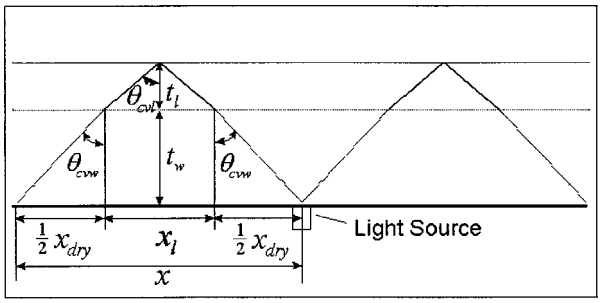


FIG. 3. Defining dimensions used in calculating liquid film thickness.

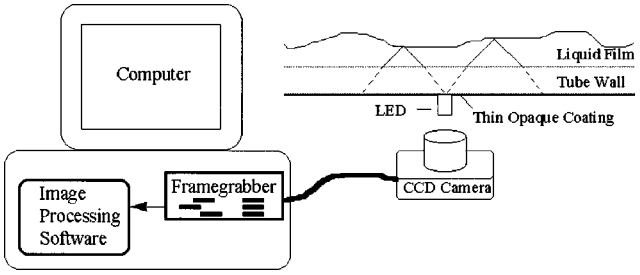


FIG. 4. Schematic of the components of the film thickness measurement system.

better approximate a point source, and to prevent light from the rear and sides of the LED from interfering with the measurement, the entire LED is painted black except for a small area directly above the light element.

The wavelength of light used may be chosen based on the availability of different light sources and the optical properties of the test section and liquid to be measured. No inherent wavelength dependence exists in the measurement method itself. LED sources emitting light ranging from green to near infrared have been used successfully with water in acrylic and polyvinyl chloride test sections.

Another possibility for a light source is a low-power laser focused to a small spot. While this has an advantage of high brightness, some disadvantages include difficulty in delivering the spot to the wall without interfering with the camera's view of the reflected light, and increased uncertainties due to vibrations of the laser source, optics, camera, and test section.

Light generated by an LED is assumed to be randomly polarized. If the Fresnel equations, Eqs. (1) and (2), are used to plot the total percentage of light reflected for each mode of propagation versus the angle of incidence, the plot would indicate a much steeper rise in reflectance near the critical angle for light traveling with the transverse magnetic mode. Ideally, then, the use of light with this polarization should yield a better signal when the image of the reflected light is analyzed for the point of greatest slope in the intensity profile. Satisfactory results have been obtained with a simple LED arrangement, however, without regard to the polarization of the emitted light.

A thin, light, semiopaque coating is applied to the outer wall of the test section at the location where film thickness is to be measured. The coating need only be large enough to completely cover the area through which reflected light could pass, typically spanning less than 4 cm. This coating homogenizes the light leaving the LED and helps to distribute light diffusely. The coating also serves to couple the light out of the wall and scatter it so that an image of the reflected light may be detected. Since most, if not all, of the light reflected from the vapor–liquid interface will arrive at the outer wall surface with an angle greater than the critical angle for the air–wall interface, without the coating, the light would reflect back into the wall and thus remain trapped there. In this particular setup, thin, frosted, plastic tape with a white adhesive is used.[43]

White spray paint has been used successfully for the semiopaque coating. The disadvantages of this are its graininess, permanence, and the difficulty in generating an even coating. As an alternative, white spray paint has been applied to a thin sheet of clear plastic, and this plastic sheet placed on the test section with a thin layer of water or oil between them to act as an optical coupling. Finally, opalized or ground glass used as a window into a test section also works well with this method.

A video camera positioned near the test section can be used to capture the reflected light image for further analysis. In this implementation, a small, inexpensive, monochrome charge-coupled device (CCD) camera[44] is mounted together with the LED in a single unit which can be positioned at any location on the test section. The video camera output is captured and digitized by a framegrabber peripheral[45] and selected frames of video are stored in the host computer's memory. The image can then be manipulated and enhanced by image processing software.

### D. Image processing algorithm

As presented earlier, locating the first fully reflected light ray is achieved by determining the point of greatest slope in the light intensities generated by the reflected rays. The point of greatest slope in the light intensity profile is found through several image processing steps. First, if a standard video signal is used (NTSC or PAL), the image must be split into two images, one composed of the even lines and one of the odd lines of the original image. This is necessary due to the interlaced video generated by standard video equipment. The odd and even lines in the video data are imaged $\frac{1}{60}$th of a second apart and therefore are representative of entirely different liquid surface structures. Both the odd and even images may be processed separately to provide two data points for each frame of video acquired.

The image manipulations are demonstrated in Figs. 5 and 6. Figure 5 shows an actual image of a portion of the light reflected from the surface of a moving liquid film. The pixel intensity values for a single row, row 50, have been extracted and plotted below the original image. Figure 6 shows how the processed intensity profile changes with each processing step. The original intensity profile is shown in each plot for comparison.

First, brightness contrast is enhanced to increase the signal-to-noise ratio [Fig. 6(a)] and a low pass filter is applied to the image to lessen random high frequency noise [Fig. 6(b)]. A gradient filter is applied [Fig. 6(c)], and the pixels with the largest gradient value are then selected [Fig. 6(d)]. Finally, if the maximum slope occurs at more than one position along the curve, a single pixel position is determined by assuming that the mean of these positions is the point where the first fully reflected ray is detected [Fig. 6(e)]. Detailed explanations of these image processing steps may be found in the work by Shedd,[41] with additional useful information in books by Russ,[46] Gonzales and Woods,[47] and Crane.[48]

This process is repeated for every row of the image, resulting in a curve representing a section of the ring of first fully reflected light rays. Figure 7 shows the result of pro-

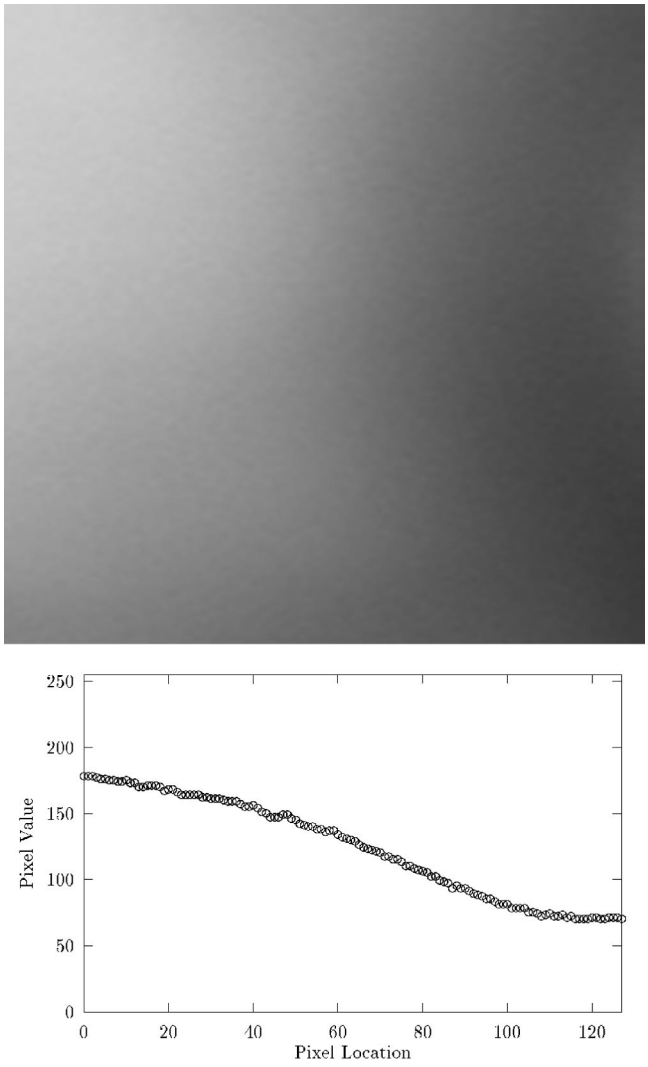


FIG. 5. Processing one row of an image. The pixel intensities from row 50 of the top image have been extracted and plotted. This pixel intensity profile will be processed as an example of the processing performed to locate the position of the first fully reflected ray.

cessing each row of the image that has been used as an example in this discussion.

### E. Defining physical distances

A narrow region of the reflected light image is analyzed as described above to determine the distance between the light source and the first fully reflected light rays. This narrow region is selected to be small enough such that curvature effects due to the circular light ring and round test section wall may be ignored. Yet the region should be large enough to help average out random noise and small, unsteady, disturbances. The analyzed image will ideally result in a vertical line of pixels at some point in the image representing the location of the reflected light rays. However, in turbulent vapor-liquid flows, the processed reflection data may not generate a straight line due to vapor bubbles, the passage of a disturbance wave, or poor contrast in the image. Fouling or dust may cause minor distortions in the final image as well. Figure 8 shows a typical processed image containing the reflection patterns from two light sources. The pattern on the left is relatively straight and its average pixel location can be used to estimate the distance between the light source and the fully reflected light rays. The pattern on the right, however, shows evidence of some significant flow disturbance; perhaps a sharp wave front or bubble.

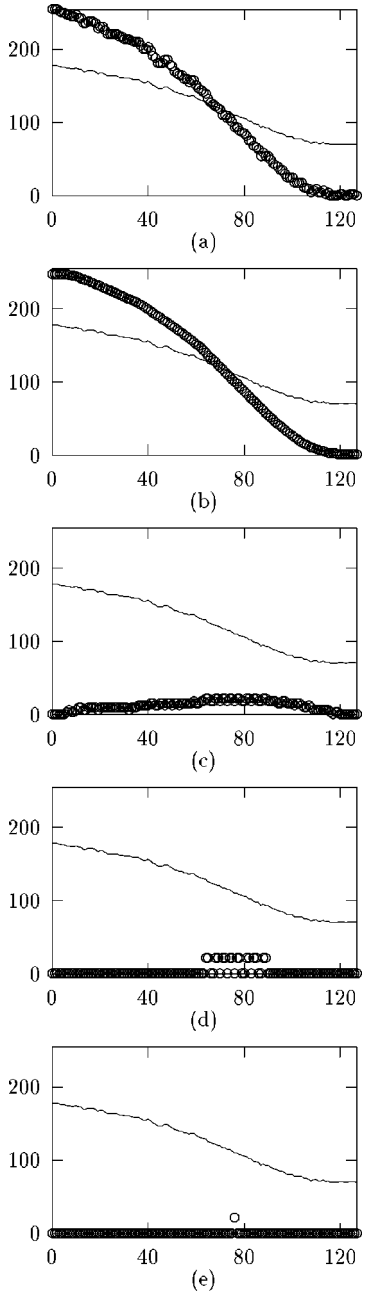


FIG. 6. Image processing steps: (a) contrast enhancement, (b) low-pass filtering, (c) gradient, (d) locating points of maximum gradient, (e) locating central point of maximum gradient.

It is necessary, then, to use a robust algorithm for determining the horizontal location of the reflected light rays. To begin with, the mean horizontal pixel location, $\overline{x}$, is determined for the set of pixels and the standard deviation, $\sigma_{\mathrm{pix}}$, about this mean is calculated.

Next, a deviation term is calculated for each pixel based on its location with respect to the mean location:

$$\eta_{\mathrm{pix}} = 1 - \frac{|x_{\mathrm{pix}} - \overline{x}|}{4(1+\sigma_{\mathrm{pix}})}. \tag{5}$$

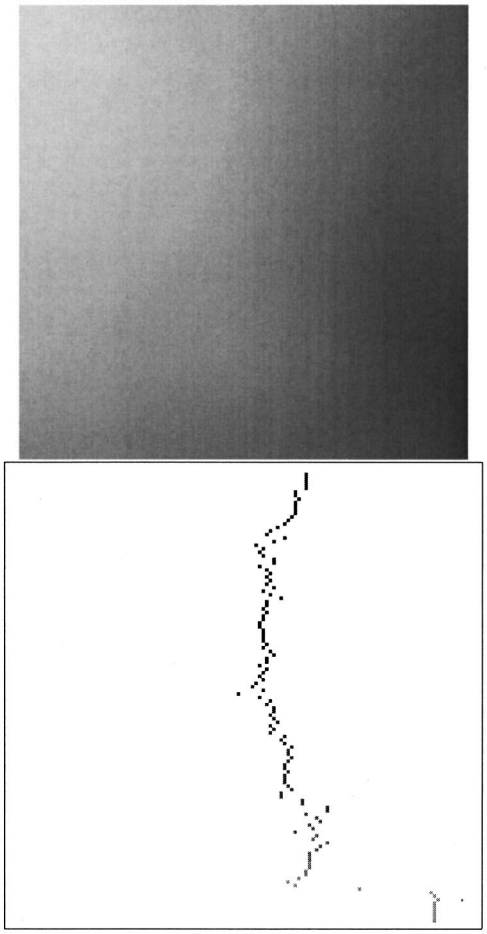

FIG. 7. The image on the right is a result of processing each row of the image on the left as described in the text.

If $\eta_{\text{pix}}<0$, it is redefined to be equal to 0. This definition attempts to compensate for variations in the individual pixel locations by giving a smaller value to pixels which lie far from the mean.

The horizontal location that will be defined as the point at which the first fully reflected rays strike the outer wall, $x_{\text{ref}}$, is calculated by a weighted average of pixel locations:

$$x_{\text{ref}}=\frac{\Sigma\,\eta_{\text{pix}}x_{\text{pix}}}{\Sigma\,\eta_{\text{pix}}}. \tag{6}$$

Finally, a confidence value is assigned to the calculated location. This takes into account the size of the standard deviation with respect to the total width of the image to help eliminate data that are badly scattered or bimodal.

$$C=\frac{\Sigma\,\eta_{\text{pix}}}{N}\left(\frac{\text{image width}-\sigma_{\text{pix}}^3}{\text{image width}}\right), \tag{7}$$

where $N$ is the number of different pixel locations averaged together. If $C<0$, it is redefined to be equal to 0.

At this point, the distance between the source and the reflected light, $x$ in Eq. (4), can be calculated from

$$x=(x_{\text{ref}}-x_o)p_{\text{scale}}+x_{\text{dry}}, \tag{8}$$

where $x_o$ is the location of the reflection of light from a dry wall surface, $p_{\text{scale}}$ is the pixel scale factor, and $x_{\text{dry}}$ is the distance between the dry reflection point and the light source. $x_o$, $p_{\text{scale}}$, and $x_{\text{dry}}$ are determined by the calibration procedure described in Sec. III. The film thickness, $t_l$, is then calculated from Eq. (4).

Due to the automated nature of the measurement, several hundred film thickness readings at a single location may be taken in a few minutes. The values determined for each measurement are written to a data file along with their respective confidence values. When the results of several measurements are averaged together, the confidence number is used as a weight so the measurements from less scattered data will have more influence in the final result. This is calculated as

$$\bar{t}_l=\frac{\Sigma_i C_i(t_l)_i}{\Sigma_i C_i}, \tag{9}$$

where the $C_i$ are the confidence values corresponding to the measured data points, $(t_l)_i$.

Through the use of large numbers of instantaneous film thickness measurements, the mean film thickness, $\bar{t}_l$, may be estimated with an accuracy of microns, even though the actual measurement resolution may be tens of microns. For instance, the data presented in Sec. IV were gathered with a system that had a pixel resolution of 0.087 mm/pixel. However, using about 600 data points, $\bar{t}_l$ was estimated to be, in one instance, 0.168+/-0.006 mm. This 99% statistical confidence interval is determined by

$$\delta_l=z_0\{\sigma_{\bar{t}_l}\}=2.58\left\{\sqrt{\frac{\Sigma_i\{C_i[(t_l)_i-\bar{t}_l]\}^2}{[\Sigma_i C_i]^2}}\right\}, \tag{10}$$

where $z_0=2.58$ is the 99% confidence coefficient and $\sigma_{\bar{t}_l}$ is an estimate of the standard error, or an estimate of the standard deviation of the set of all mean values of all possible sample sets of this size.[49]

## III. CALIBRATION

Several details about the measurement apparatus and optical properties of both the test section wall and test liquid need to be known before physical distances can be calculated. An automated calibration procedure has been developed to determine the following parameters: the pixel scale factor (mm/pixel), the index of refraction of the test section wall material ($n_w$), the index of refraction of the liquid ($n_l$), the test section wall thickness ($t_w$), and the distance between the light source and its first ray completely reflected from a dry surface ($x_{\text{dry}}$).

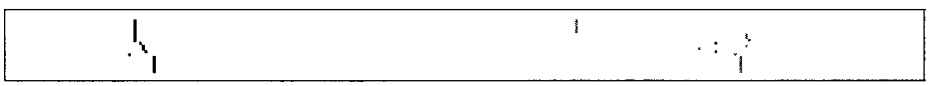

FIG. 8. This image shows the processed surface reflection patterns from two light sources. The patterns represent points on the liquid surface separated by about 26 mm.

### A. Obtaining the pixel scale factor

Among the most critical parameters needed is the pixel scale factor which relates a physical dimension to the pixel size. It is determined by the lens system of the camera, the size of the CCD array inside the camera, and the distance between the camera and the test section wall. To obtain a value of the scale factor for a given setup, a reference material of known thickness and composition is used to generate a reflection pattern whose dimensions may be calculated quite accurately from

$$x_{\mathrm{cal}} = 4t_w \tan(\theta_{cvw}), \tag{11}$$

where $x_{\mathrm{cal}}$ is the distance between two sides of the reflected light ring ($2x$ in Fig. 3). The image processing algorithm described above is used to determine the number of pixels between the two sides of the reflected light ring and the pixel scale factor is then calculated.

$$p_{\mathrm{scale}} = \frac{x_{\mathrm{cal}}}{\text{pixel distance}}. \tag{12}$$

The pixel scale factor needs only to be determined once for a given camera/LED setup. The factor has been found to be very consistent, even after moving and remounting the camera apparatus several times. It is important, however, that the camera be mounted quite rigidly with respect to the test section wall to maintain a constant pixel scale factor.

### B. Determining the unknown properties of the test section and liquid

Before any measurement or further calibration can be performed, the dry wall reference positions of the reflected light ring must be determined. This is done by mounting the light source and camera at the desired measurement location. With no liquid on the wall, several images of the reflected light ring are processed and averaged to give $x_{\mathrm{dry}}$ of Eq. (4).

With the dry wall reference positions known, the unknown properties of the test section and test fluid can be determined. Beginning with the simplest case, if either the index of refraction of the wall material, $n_w$, or the wall thickness, $t_w$, is known, the other value may be calculated from

$$x_{\mathrm{dry}} = 2t_w \tan(\theta_{cvw}), \tag{13}$$

where $\theta_{cvw} = \sin^{-1}(1/n_w)$.

If, however, both $t_w$ and $n_w$ are unknown while the index of refraction of the liquid, $n_l$, is known, or $n_l$ is unknown while the other two are known, some knowledge of the light interaction with both the fluid and the wall material must be obtained. To do this, liquid is introduced in the test section so that its level exceeds

$$t_{tl} = \frac{t_w(\tan\theta_{clw} - \tan\theta_{cw})}{\tan\theta_{cl}}. \tag{14}$$

In this case, the light reflected from the liquid surface returns to the outer wall surface at a distance greater than that of the light reflected from the liquid–wall interface and the image of the rays reflected from the liquid–wall interface becomes visible. Several images of this reflection pattern are processed and averaged to determine the distance between the light source and the edge of the reflected light ring, $x_{\mathrm{liq}}$.

Now, Eq. (13), together with

$$x_{\mathrm{liq}} - x_{\mathrm{dry}} = 2t_w(\tan\theta_{clw} - \tan\theta_{cvw}) \tag{15}$$

and

$$n_l = \frac{\sin\theta_{clw}}{\sin\theta_{cvw}}, \tag{16}$$

give three equations relating the quantities $t_w$, $n_l$, $\theta_{clw}$, and $\theta_{cvw}$. Thus, if one of these is given, the other three may be determined. Solving for $t_w$ or $n_w$ from Eq. (13) is quite simple if one of these values is known. If only $n_l$ is known, however, Eqs. (13), (15), and (16) need to be solved simultaneously for three unknowns. One efficient means for numerically solving these equations is via the regula falsi method.[50]

Experience has shown that a dry wall calibration should be performed with each new camera placement. This includes finding the new dry wall reflection positions and determining a new wall thickness using the value of $n_w$ determined by one of the methods previously described. Essentially, this serves to ''zero'' the measurement system at each wall location.

This calibration procedure can also be used to determine the indices of refraction of a solid or liquid that does not significantly scatter or absorb the light generated by the light source. In addition, this method can be used to determine the thickness of clear materials, and even to find the relative angle between two surfaces of a clear material if one surface has a fairly linear slope with respect to the other.[41]

## IV. EXPERIMENTAL RESULTS

### A. Static liquid measurements

Static liquid measurements have been taken and compared with measurements made by the needle-contact method. These results are shown in Fig. 9. The average difference between measurements by the two methods is 2.2%.

### B. Flowing film measurements

Mean liquid film thickness measurements have been taken for two-phase, annular flow in two different tube geometries. The basic flow apparatus is described in the thesis by Shedd.[41] Figure 10 compares data collected using this technique with that presented by Fukano and Ousaka,[5] as well as Hurlburt and Newell.[40] Although the flow conditions vary between data sets, the data measured with the automated system follow the trends of the other researchers well. An asymmetric peak in film thickness has not been measured previously, possibly due to the difficulty of obtaining these measurements with other techniques, but possibly because this asymmetry is introduced by the current experimental apparatus. Data presented by Dallman[1] indicate some asymmetry, though he only provides one additional radial point beyond the vertical axis.

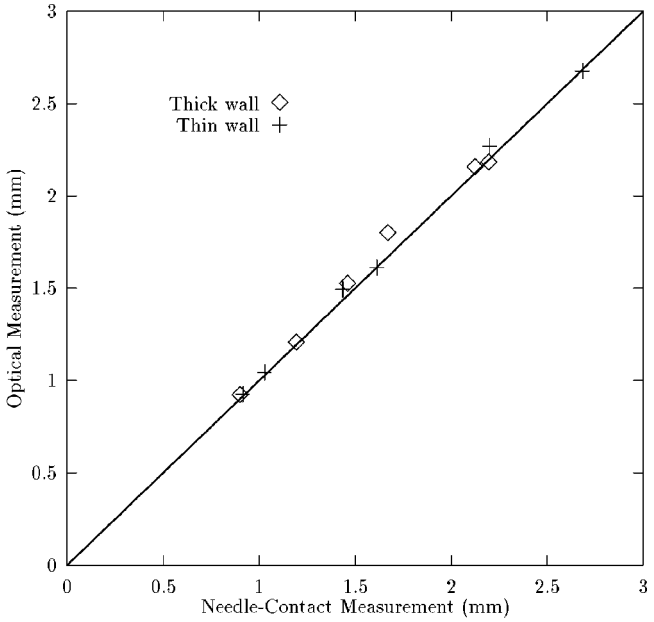


FIG. 9. Plot of static film thickness measured optically vs those measured by needle contact. Measurements were made using wall thicknesses of 2.95 (thin wall) and 6.47 mm (thick wall).

Figure 11 is a plot of the film profile along the four walls of a square tube for a single flow condition. Figure 12 shows the change in thickness of the film on each wall as flow conditions change.

## V. EXPERIMENTAL ERROR

Error in an instantaneous measurement may come from several sources: electronic noise, vibrational noise, relatively large disturbances in the film, poor contrast in the image, and camera movement with respect to the light source.

The effects of electronic and vibrational noise, as well as large film disturbances, are minimized through the use of large numbers of data samples. Electronic noise is introduced at the camera with thermal current fluctuations in the CCD

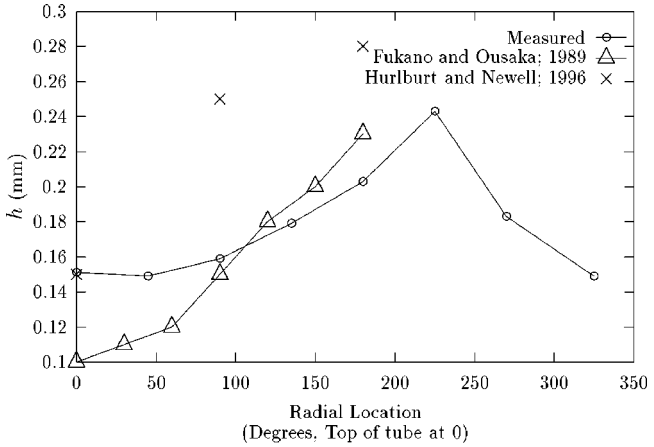


FIG. 10. The film thicknesses measured around the test section are plotted together with representative data from the literature. The measured flow conditions are $\dot{m}_a = 0.021$ and $\dot{m}_l = 0.019$ kg/s. The Fukano and Ousaka data is taken from a flow with $\dot{m}_a = 0.025$ and $\dot{m}_l = 0.019$ kg/s. Hurlburt and Newell measured a flow with $\dot{m}_a = 0.020$ and $\dot{m}_l = 0.013$ kg/s.

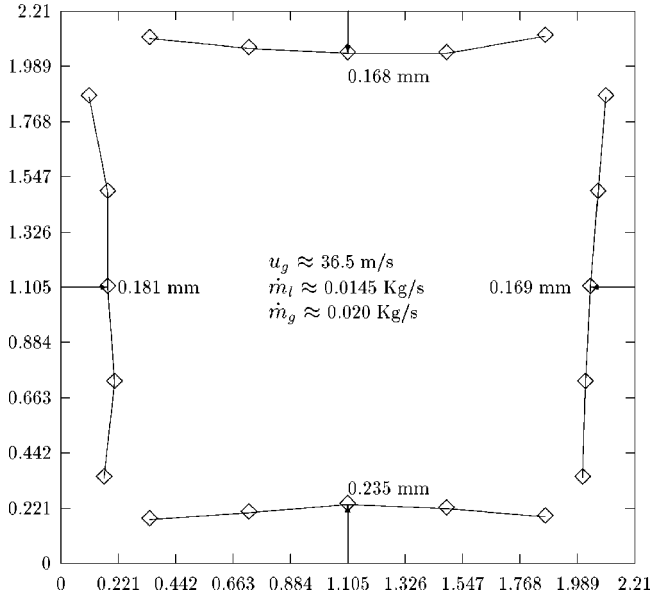


FIG. 11. Film thickness profile for a tube of square cross section. Length of tube sides are 2.21 cm.

array and with the loss of information when the CCD data is converted to the NTSC standard analog signal. Noise is added to the video signal as it travels from the camera to the framegrabber board, and when information is lost as the analog signal is converted to an 8-bit digital signal and stored in memory. Vibrational noise consists primarily of vibrations of the camera, light source, and tube wall with respect to each other. While the apparatus is mounted securely to the tube, relative vibrational amplitudes on the order of the precision of the measurement ($\approx 10\ \mu$m) are quite possible. The presence of electronic and vibrational noise is evidenced by the nonzero standard deviation that exists for calibration measurements of a tube wall with no liquid flow. Measurements indicate that most of this noise is on the order of one pixel in amplitude ($\sigma = 0.487$). After about 300 data points, however, the expected value of the location of the reflected light may be determined with 99% statistical confidence to a precision of 0.08 pixels, indicating that the noise is primarily random in nature.

Noise due to film disturbances may be indicated by the

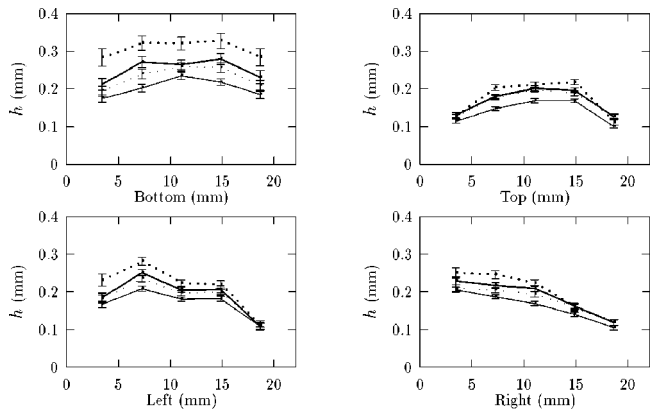


FIG. 12. These plots show the change in mean film thickness as flow conditions are changed for the square tube plotted in Fig. 11.

standard deviations in the film data ranging from about 1 pixel to nearly 3 pixels. Not only do structures such as large waves and vapor bubbles cause fluctuations in the measured film thickness, but a sloping of the surface of as little as 5° can lead to errors of several hundred percent. Several researchers have studied the liquid surface in vapor–liquid flows,[14,30,51–53] and these results indicate that the liquid film surface is fairly smooth and parallel to the wall for very thin films ($>1$ mm), with surface roughness increasing for thicker films ($\approx 5$ mm). In addition, as shown by Paras and Karabelas,[52] wave surface slopes are generally less than 3°. Thus, this measurement method is best suited for films less than about 1 mm thick. However, with liquid film structures typically moving at velocities greater than 1 m/s, the image that is analyzed is actually a time average of reflections generated by the fluid surface during the time the shutter is open, and this seems to allow for accurate results in thicker films with wavy surfaces.

Some error has been detected when background light or source brightness varies. This error is generally on the order of 1 to 3 pixels and is suspected to be caused by the brightness nonlinearities in the camera and framegrabber video processing electronics. Careful adjustment of the camera gamma parameter can minimize these nonlinearities. In practice, a light-blocking box is mounted around the camera and test section at the measurement point to keep changes in background light to a minimum.

Errors due to camera movement have been virtually eliminated by using two surface reflections as indicated in the setup shown in Fig. 4. With this configuration, film thicknesses are calculated using the reflected light images on both sides of the light source, then averaged together. The effect of any shift of the camera with respect to the light source is then canceled between the data from the two sides.

## ACKNOWLEDGMENTS

This work was supported by the Air Conditioning and Refrigeration Center at the University of Illinois at Urbana-Champaign, a National Science Foundation industry/university cooperative research center.

[1] J. C. Dallman, Ph.D. thesis, University of Illinois at Urbana-Champaign, Urbana, IL, 1978.
[2] J. E. Laurinat, Ph.D. thesis, University of Illinois at Urbana-Champaign, Urbana, IL, 1982.
[3] G. F. Hewitt, in *Handbook of Multiphase Systems*, edited by G. Hetsroni (McGraw–Hill, New York, 1982), pp. 10-67–10-85.
[4] K. Sekoguchi, A. Ousaka, T. Fukano, and T. Morimoto, Bull. JSME **25**, 1559 (1982).
[5] T. Fukano and A. Ousaka, Int. J. Multiphase Flow **15**, 403 (1989).
[6] M. Miya, Ph.D. thesis, University of Illinois at Urbana-Champaign, Urbana, IL, 1970.
[7] M. W. E. Coney, J. Phys. E **6**, 903 (1973).
[8] R. C. Brown, P. Andruessi, and S. Zanelli, Can. J. Chem. Eng. **56**, 754 (1978).
[9] J. P. Villeneuve and Y. Ouellet, Rev. Sci. Instrum. **49**, 1425 (1978).
[10] J. E. Laurinat, Master's thesis, University of Illinois at Urbana-Champaign, Urbana, IL, 1979.
[11] N. Andritsos, Ph.D. thesis, University of Illinois at Urbana-Champaign, Urbana, IL, 1985.
[12] B. J. Azzopardi, Nucl. Eng. Des. **92**, 121 (1986).
[13] W. S. Bousman, J. B. McQuillen, and L. C. White, Int. J. Multiphase Flow **22**, 1035 (1996).
[14] S. Jayanti, G. F. Hewitt, and S. P. White, Int. J. Multiphase Flow **16**, 1097 (1990).
[15] T. D. Karapantsios, S. V. Paras, and A. J. Karabelas, Int. J. Multiphase Flow **15**, 1 (1989).
[16] Y. Hagiwara, K. Suzuki, and T. Sato, Memoirs of the Faculty of Engineering, Kyoto University **44**, 309 (1982).
[17] Y. Hagiwara, E. Esmaeilzadeh, H. Tsutsui, and K. Suzuki, Int. J. Multiphase Flow **15**, 421 (1989).
[18] E. M. A. Hussein and P. J. Ingham, in *Measurement Techniques in Multiphase Flows*, of The Proceedings of the ASME Fluids Engineering Division, Vol. 244, edited by T. J. O'Hearn *et al.* (The American Society of Mechanical Engineers, New York, 1997), pp. 347–356.
[19] S. L. Ceccio, in *Experimental Techniques in Multiphase Flows*, of The Proceedings of the ASME Fluids Engineering Division, Vol. 25, edited by T. J. O'Hearn and R. A. Gore (The American Society of Professional Engineers, New York, 1991), pp. 1–8.
[20] M. R. Özgü and J. C. Chen, Rev. Sci. Instrum. **44**, 1714 (1973).
[21] R. K. Sun, W. F. Kolbe, B. Leskovar, and B. T. Turko, IEEE Trans. Nucl. Sci. **NS-29**, 688 (1981).
[22] R. K. Sundaram, J. C. Chen, E. J. London, and N. Eberhardt, in *Proceedings of the 27th International Instrumentation Symposium*, ISA Aerospace Industry Division and ISA Test Measurement Division (ISA, Research Triangle Park, NC, 1981), pp. 299–312.
[23] B. T. Turko, W. F. Kolbe, B. Leskovar, and R. K. Sun, IEEE Trans. Nucl. Sci. **NS-28**, 728 (1981).
[24] M.-H. Chun and C.-K. Sung, Int. J. Multiphase Flow **12**, 627 (1986).
[25] F. Klug and F. Mayinger, Nucl. Eng. Des. **146**, 35 (1994).
[26] X. Chen, T. Butler, and J. P. Brill, in *HTD, Proceedings of the ASME Heat Transfer Division at the International Mechanical Engineering Congress and Exposition* (American Society of Mechanical Engineers, New York, 1996), Vol. 3, pp. 201–208.
[27] G. E. Thorncroft and J. F. Klausner, Trans. ASME: J. Fluids Eng. **119**, 164 (1997).
[28] J. F. Klausner, L. Z. Zeng, and D. M. Bernhard, Rev. Sci. Instrum. **63**, 3147 (1992).
[29] J. D. Barter and P. H. Y. Lee, Appl. Phys. Lett. **64**, 1896 (1994).
[30] T. Sattelmayer, K. H. Sill, and S. Wittig, Technisches Messen **54**, 155 (1987).
[31] J. Himmelsbach, B. Noll, and S. Wittig, Int. J. Heat Mass Transf. **37**, 1217 (1994).
[32] H. Müller *et al.*, MTZ: Motortechnische Zeitschrift **55**, 220 (1994).
[33] R. P. Roy, J. Ku, I. Kaufman, and J. Shukla, Rev. Sci. Instrum. **57**, 952 (1986).
[34] R. L. Schmitt, W. H. Stevenson, and H. C. Stevenson, in *Proceedings of the Inspections, Measurement and Control Symposium, International Congress of Applications of Lasers and Electro-Optics 1982* (Laser Institute of America (LIA), Boston, MA, 1982), Vol. 33, pp. 31–35.
[35] D. I. Driscoll, R. L. Schmitt, and W. H. Stevenson, Trans. ASME: J. Fluids Eng. **114**, 107 (1992).
[36] J. E. R. Coney, E. A. M. El-Shafei, and C. G. W. Sheppard, Opt. Lasers Eng. **11**, 1 (1989).
[37] C. F. Than, K. C. Tee, K. S. Low, and C. P. Tso, Smart Mater. Struct. **2**, 13 (1993).
[38] S. C. M. Yu, C. P. Tso, and R. Liew, Appl. Math. Modelling **20**, 540 (1996).
[39] L. W. Evers and K. J. Jackson, in *Electronic Engine Controls 1995*, SAE Technical Paper Series, Vol. SP-1082 (Society of Automotive Engineers, Warrendale, PA, 1995), pp. 1–7, reprint, number 950002.
[40] E. T. Hurlburt and T. A. Newell, Exp. Fluids **21**, 357 (1996).
[41] T. A. Shedd, Master's thesis, University of Illinois at Urbana-Champaign, Urbana, IL, 1998.
[42] W. Mathews, Personal communication, Department of Mechanical and Industrial Engineering, University of Illinois at Urbana-Champaign, 1998.
[43] Lepages Freezer Tape, Lepages, Inc., 120 Delta Drive, Pittsburgh, PA 15238-2806.
[44] CCD Camera Model 150931, Jameco, 1355 Shoreway Rd., Belmont, CA 94002.
[45] TargaPlus Video Framegrabber, Truevision, Inc., 2500 Walsh Avenue, Santa Clara, CA 95051.
[46] J. C. Russ, *The Image Processing Handbook* (Chemical Rubber, Boca Raton, FL, 1994).
[47] R. C. Gonzalez and R. E. Woods, *Digital Image Processing*, 3rd ed. (Addison–Wesley, Reading, MA, 1992).

[48] R. Crane, *A Simplified Approach to Image Processing*, 1st ed. (Prentice Hall, Upper Saddle River, NJ, 1997).
[49] J. Mandel, *The Statistical Analysis of Experimental Data* (Dover, New York, 1984).
[50] F. Scheid, *Numerical Analysis, Schaum's Outline Series*, 2nd ed. (McGraw–Hill, New York, 1988).
[51] G. F. Hewitt, S. Jayanti, and C. B. Hope, Int. J. Multiphase Flow **16**, 951 (1990).
[52] S. V. Paras and A. J. Karabelas, Int. J. Multiphase Flow **17**, 439 (1991).
[53] T. Hibiki, K. Mishima, and A. Tsuruno, in *Flow Visualization and Image Processing of Multiphase Systems*, The Proceedings of the ASME Fluids Engineering Division, Vol. 209, edited by W. J. Yang, F. Yamamoto, and F. Mayinger (The American Society of Mechanical Engineers, New York, 1995), pp. 243–250.